Droplet Deposition and Momentum Transfer in Annular Flow

Larry B. Fore and Abraham E. Dukler
Dept. of Chemical Engineering, University of Houston, Houston, TX 77204

Entrainment and deposition in gas–liquid annular upflow are known to account for as much as 20% of the pressure gradient, through droplet accelerations in the core region. Momentum is transferred from the core when droplets decelerate upon impact with the liquid film. It is usually assumed that all of this momentum is transferred to the film, essentially driving the film upward in conjunction with interfacial friction. New data, obtained for annular gas–liquid upflow in a 5.08-cm-ID tube, are used in a momentum balance analysis to determine the mechanism of momentum transfer from depositing droplets. Measurements include the liquid film thickness, wall shear stress, pressure gradient, entrained liquid fraction, droplet deposition rate, droplet centerline axial velocity, and mass-average drop size for two gas–liquid systems. This analysis supports the idea that large droplets displace the film locally and decelerate primarily at the wall, effectively transferring negligible momentum to the liquid film.

Introduction

Gas–liquid annular flow in a tube is characterized by the flow of a thin, wavy liquid film along the wall, with a core of gas flowing in the center of a tube. At gas velocities slightly above the flooding condition, film-churning occurs, with the liquid film at any given position moving up or down, with the net flow upward. As the gas velocity is increased, large-amplitude flow surges appear on the film (Hall-Taylor et al., 1963; Nedderman and Shearer, 1963). These disturbance waves, noted as a key mechanism for heat and mass transfer (Dukler, 1977), are characterized by a coherent upward motion over several tube diameters. Above a critical liquid flow rate, a significant portion of the input liquid feed can exist as droplets entrained in the gas core. The droplets form from the disturbance waves, accelerate in the gas core, and deposit back onto the film, eventually reaching an equilibrium where the rates of entrainment and deposition are approximately equal and constant. The process of droplet interchange increases the overall pressure drop of the system and enhances heat and mass transfer above that expected in single-phase flows.

Gas–liquid annular flow occurs in enough variety in important situations to warrant continued improvement in predictions of such quantities as pressure gradient and heat-and mass-transfer rates. Unfortunately, existing correlations are accurate only near the conditions from which they were developed. At the present time, a better understanding of the mechanisms by which momentum, heat, and mass are transported is needed to develop more general relations. Droplet interchange is important in this respect, having been demonstrated to account for as much as 20% of the pressure gradient (Moeck and Stachiewicz, 1972; Lopes and Dukler, 1986; Schadel and Hanratty, 1989).

It is well-understood that entrainment adds to the pressure gradient through the acceleration of droplets by the gas core. When a droplet deposits, it is usually assumed that all of the momentum carried by that droplet is transferred to the liquid film. Under this view, the total interfacial force that drives the film upward is composed of two distinct parts, frictional forces exerted by the gas flow field and forces generated as depositing droplets decelerate. Interfacial friction is distributed continuously over the interface, while droplets deposit at discrete locations that may represent only a fraction of the total interfacial area. The intent of this study is to determine how momentum is transferred from depositing droplets, and whether deposition should be considered a simple addition to interfacial friction. To achieve this, experiments have been performed using two gas–liquid systems in a 5.08-cm-ID tube at pressures slightly above atmospheric, for gas velocities ranging from film-churning well into the regime of disturbance waves. A momentum balance analysis and physical arguments are then used to develop a new insight into the deposition process.

Correspondence concerning this article should be addressed to L. B. Fore.
A. E. Dukler died in February 1994.

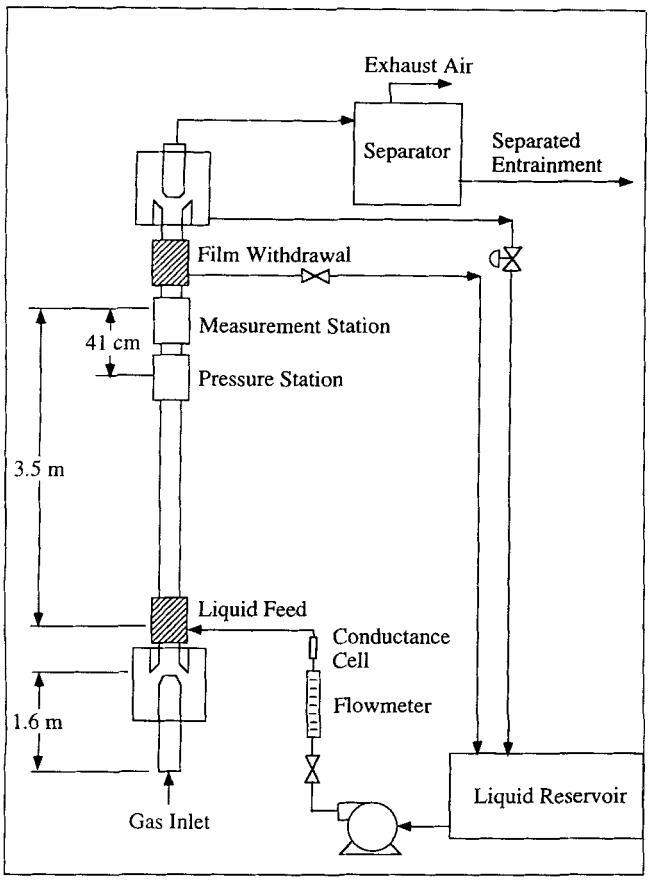

Figure 1. Vertical multiphase flow loop.

Experimental

Flow loop

The flow loop used in this study is shown in Figure 1. It consists of a vertical column, constructed of 5.08-cm-ID clear acrylic tubing and configured for annular upflow. Metered air was introduced at the bottom, 1.6 m below the liquid feed device. The feed device, constructed of porous steel, enabled the introduction of the liquid as a thin annular film. A measurement station for film thickness, wall shear stress, and pressure was located 3.5 m, or approximately 69 tube diameters, above the liquid feed. A second porous device was used to withdraw the liquid film above the measurement station. The remaining mixture of gas and droplets was then removed through a discharge tube to a gas–liquid separator, where the separated entrainment could be measured. All liquid was recycled to the feed reservoir, where the temperature was constantly monitored at 18°C, while the air was exhausted from the system.

Measurement station and techniques

The measurement station is shown in Figure 2. A film thickness probe, wall shear stress probe, and pressure transducer were located at the same axial location, but offset from each other along the perimeter of the measurement station. A second film thickness probe was located 5.08 cm below. The two film thickness probes were used in conjunction to determine mean wave velocities with cross-correlation analyses. The mean pressure gradient was calculated with the difference between the upper transducer and a second one located 41 cm below.

Conductance wires, used in many other investigations (Miya et al., 1971; Brown et al., 1978; Zabaras et al., 1986), were used to determine the fluctuating film thickness. The film thickness probes consisted of parallel pairs of Pt-13% Rh wires, 0.076 mm in diameter and separated by 3 mm. Half of each wire was insulated so that the measurement occurred on one side of the tube. A flush-mounted, temperature-compensated hot-film probe, of the type described by Hanratty and Campbell (1983), was used to measure the fluctuating wall shear stress. The shear stress probe was secured into a

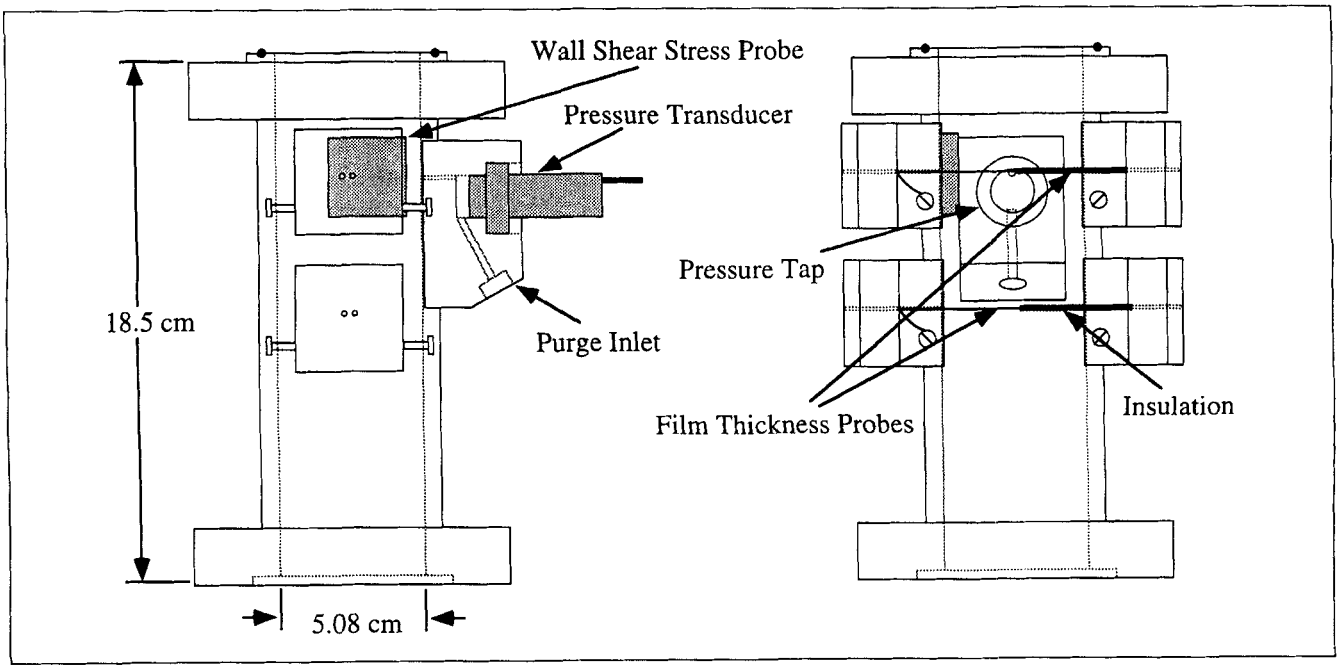

Figure 2. Measurement station for film thickness, wall shear stress, and pressure.

Table 1. Physical Properties of Test Liquids

	Viscosity (18°C)	Density (18°C)	Re_{LFC}
1-cp liquid	1.05 cp	999 kg/m^3	340
6-cp liquid	6.05 cp	1,128 kg/m^3	120

recess in the tube wall, machined specifically to ensure a configuration flush with the surrounding surface. Two Druck Model PDCR 820 pressure transducers were used to measure the pressure gradient. The taps leading into the tube from each transducer were 1 mm ID by 3 mm long. A slow, continuous purge of liquid was used to keep gas bubbles out of the pressure taps.

The entrained liquid fraction, E, and deposition mass-transfer rate, R_D, were estimated by locating a film-removal device at four axial locations: 35, 50, 73 and 91 cm below the discharge tube. Film removal suppresses drop formation, allowing only deposition over the distance between the removal device and the discharge tube. The flow rate of collected drops, W^*_{LE}, decreases as this distance increases, according to

$$\frac{dW^*_{LE}}{dz} = -\pi D R_D. \tag{1}$$

Assuming a constant deposition rate after film removal, a plot of W^*_{LE} vs. distance from the discharge tube yields an estimate of the deposition rate and equilibrium entrainment flow rate from the slope and intercept, respectively, of a fitted line. This is analogous to the film-removal technique employed by Cousins and Hewitt (1968) and others, in which the flow rate of deposited, instead of remaining, droplets is measured. These techniques provide only an estimate of the true equilibrium deposition rate, given that deposition is probably different after the film is removed.

The droplet axial velocity and size were measured with a modified version of the Semiat and Dukler (1981) laser-grating technique (Fore and Dukler, 1995). The gas–droplet slip ratio, S_R, was approximated by the ratio of the centerline mean drop velocity to the centerline mean gas velocity, which was measured with an LDA system. The critical Reynolds number for entrainment, Re_{LFC}, was determined by increasing the liquid feed rate at fixed gas velocities until droplets first appeared. Further details of the experiments and calibration methods can be found elsewhere (Fore, 1993).

Experimental conditions

Flow conditions for these experiments range from film-churning well into the regime of disturbance waves. The equilibrium assumption, where the transfer rates are equal and the entrained fraction is constant, was verified by entrainment measurements at a series of distances from the feed. At 3.5 m from the feed, the entrained fraction was uniform, within measurement error, with distance. Air and two liquids were used: water and a 50% glycerin–water mixture, with physical properties summarized in Table 1 (Miner and Dalton, 1953). The surface tension for both liquids is essentially the same, 72 and 70 dyne/cm for the 1-cp and 6-cp liquids, respectively. The boundary between film-churning and upward-traveling disturbance waves occurred around gas velocities of 19 m/s. The critical liquid Reynolds number, Re_{LFC}, was approximately independent of gas velocity at 340 and 120 for 1-cp and 6-cp systems, respectively. Gas velocities, U_{GS}, cover one condition in film-churning for each liquid Reynolds number, $Re_L = 4\Gamma/\nu$, with all others in the regime of upward-traveling disturbance waves.

Liquid feed rates were chosen to represent comparable superficial liquid velocities, U_{LS}, for the two liquids. Liquid Reynolds numbers of 56, 140, 280, 420, and 560 for the 6-cp liquid can be compared on the basis of superficial liquid velocity to 300, 750, 1,500, 2,250, and 3,000, respectively, for the 1-cp liquid.

Measurements

Tables 2 and 3 summarize the measured mean quantities of film thickness, wall shear stress, pressure gradient, wave velocity, deposition rate, entrained fraction, centerline droplet axial velocity, and mass-average drop size. Asterisks (*) are used where quantities are negligible or inapplicable, as in the case of entrained fraction and drop velocity for $Re_L = 300$ and 56. During film-churning, the entrained fraction was large, as is frequently observed (Zabaras et al., 1986; Hewitt et al., 1985), while the deposition rate was negligibly small. The severe reduction of deposition rate and entrained fraction with increasing gas velocity for $Re_L = 140$ is due to proximity to the critical Reynolds number of 120. Although the deposition measurements are probably the most unreliable, they agree reasonably well with recent measurements of Schadel et al. (1990), which used a film-tracer technique (Quandt, 1965) in different tube sizes.

The average droplet velocity at the tube centerline, V_d, is larger than the corresponding superficial gas velocity and smaller than the centerline gas velocity, with a nearly uniform slip ratio of $S_R = 0.8$. For the purpose of the following momentum transfer analysis, V_d is assumed to be the equilibrium velocity attained by depositing droplets. The wave velocity, C_w, was determined from the peak time delay of a cross-correlation between the two film thickness probes. It therefore represents an average wave velocity, weighted according to wave size, and is used to approximate the velocity at which droplets enter the gas core. Of further importance to the following analysis is the mass-average drop size, d_{30}. This is the size that best represents the momentum of individual depositing droplets. In each case, d_{30} is comparable to, and sometimes larger than, the mean film thickness. This is reasonable, considering that all drops originate from disturbance waves, which are several times larger than the mean film thickness.

Momentum Transfer Analysis

Core momentum balance

The control volume for a momentum balance on the gas–droplet core is shown in Figure 3. It is bounded radially by the gas–liquid interface and axially by two planes spaced a distance, L, apart. The diameter of the control volume is $(D - 2m)$, where D is the tube diameter and m is the mean film thickness. Droplets are ejected from the disturbance waves at the rate, R_E, with an initial axial velocity approximately equal to the mean wave velocity. They accelerate in the gas core to the mean droplet centerline axial velocity, V_d, and deposit

Table 2. Measured Quantities for the Air–Water System ($\mu_L = 1$ cp)

Re_L	ρ_G kg/m^3	U_{GS} m/s	m mm	$\bar{\tau}_w$ Pa	$-\nabla P$ Pa/m	C_w m/s	R_D kg/m^2·2s	E	V_d m/s	d_{30} mm
300	1.20	16.5	0.520	0.40	384	0.65	*	*	*	*
300	1.22	20.3	0.379	0.45	337	0.73	*	*	*	*
300	1.23	24.0	0.338	0.83	310	0.88	*	*	*	*
300	1.25	27.6	0.308	1.66	378	0.89	*	*	*	*
300	1.27	31.1	0.279	2.63	434	1.04	*	*	*	*
300	1.28	34.0	0.265	3.50	490	1.54	*	*	*	*
300	1.30	36.5	0.272	4.39	539	1.75	*	*	*	*
750	1.20	16.4	0.605	0.63	528	0.72	*	0.300	20.1	0.364
750	1.22	20.2	0.454	0.96	476	1.30	0.0124	0.232	22.7	0.329
750	1.24	23.9	0.380	1.64	461	1.54	0.0167	0.211	25.3	0.312
750	1.26	27.4	0.354	2.70	542	1.81	0.0191	0.222	28.7	0.313
750	1.28	30.9	0.320	3.85	617	2.12	0.0215	0.244	31.1	0.291
750	1.29	33.6	0.302	4.83	686	2.31	0.0233	0.268	33.4	0.280
750	1.31	36.2	0.307	5.81	772	2.42	0.0241	0.283	34.8	0.302
1,500	1.21	16.3	0.691	0.83	567	1.02	*	0.340	20.7	0.431
1,500	1.22	20.2	0.499	1.62	517	1.45	0.0235	0.302	23.2	0.370
1,500	1.24	23.8	0.459	2.53	614	1.75	0.0297	0.289	26.1	0.348
1,500	1.27	27.3	0.406	3.75	705	2.03	0.0359	0.304	29.6	0.331
1,500	1.29	30.6	0.365	5.04	789	2.21	0.0446	0.332	32.2	0.306
1,500	1.31	33.2	0.337	6.09	871	2.42	0.0532	0.360	35.0	0.304
1,500	1.33	35.6	0.339	7.14	934	2.54	0.0570	0.375	36.2	0.307
2,250	1.21	16.3	0.786	1.11	712	1.00	*	0.340	20.8	0.571
2,250	1.23	20.1	0.584	2.19	657	1.45	0.0256	0.321	23.5	0.460
2,250	1.25	23.7	0.518	3.32	756	1.81	0.0350	0.319	26.7	0.420
2,250	1.27	27.1	0.450	4.72	859	2.12	0.0460	0.337	30.3	0.389
2,250	1.30	30.4	0.402	6.16	950	2.31	0.0553	0.360	32.9	0.388
2,250	1.32	32.8	0.369	7.31	1,049	2.54	0.0628	0.381	35.8	0.397
2,250	1.35	35.1	0.372	8.52	1,129	2.67	0.0669	0.394	37.5	0.379
3,000	1.22	16.2	0.890	1.32	838	1.21	*	0.350	20.9	0.662
3,000	1.24	20.0	0.643	2.64	798	1.59	0.0443	0.340	23.8	0.590
3,000	1.25	23.7	0.572	4.03	889	1.81	0.0534	0.342	27.3	0.518
3,000	1.28	26.9	0.496	5.52	994	2.21	0.0619	0.356	30.9	0.493
3,000	1.31	30.0	0.443	7.04	1,100	2.42	0.0689	0.370	33.5	0.499
3,000	1.34	32.5	0.405	8.38	1,194	2.54	0.0811	0.389	37.0	0.475
3,000	1.37	34.6	0.405	9.76	1,273	2.67	0.0848	0.397	37.9	0.477

onto the liquid film at the rate, R_D. Equilibrium flow is assumed, so that the time-averaged entrainment flow rate is constant through the control volume and $R_E = R_D$.

The time-average axial momentum balance over this control volume is written

$$\int_A U_z \rho U_z \, dA = \int_A T_z \, dA + \int_V B_z \, dV, \tag{2}$$

where U_z, ρ, T_z, and B_z are mean local values of axial velocity, density, axial surface force, and axial body force, respectively. The contribution to the convective integral comes from the entrainment–deposition process, where slow-moving droplets enter and fast-moving droplets leave the control volume through the interface. Using $R_E = R_D$, the convective integral becomes

$$\int_A U_z \rho U_z \, dA = \pi(D-2m)LR_D(V_d - C_w). \tag{3}$$

The surface force integral is

$$\int_A T_z \, dA = -\pi(D-2m)L\tau_i - \pi\frac{(D-2m)^2}{4}\Delta P, \tag{4}$$

where τ_i is the mean interfacial stress and ΔP is the mean pressure drop over the distance, L. The body force integral is evaluated with the droplet concentration, $C_E = \rho_G S_R W_{LE}/W_G$, and the gravitational acceleration, g, as

$$\int_V B_z \, dV = -(\rho_G + C_E)g\frac{\pi(D-2m)^2}{4}L. \tag{5}$$

The axial momentum balance on the gas core is then rearranged to give

$$-\frac{\Delta P}{L} = \left\{\frac{4}{(D-2m)}\tau_i\right\} + \{g(\rho_G + C_E)\} + \left\{\frac{4}{(D-2m)}R_D[V_d - C_w]\right\}. \tag{6}$$

It is convenient to consider the bracketed terms as three components of the total pressure gradient as

$$\nabla P_T = \nabla P_I + \nabla P_C + \nabla P_E. \tag{7}$$

where ∇P_T is the mean pressure gradient acting on the control volume, ∇P_I is the pressure gradient due to interfacial

Table 3. Measured Quantities for the Air–50% Glycerin–Water System (μ_L = 6 cp)

Re_L	ρ_G kg/m^3	U_{GS} m/s	m mm	$\overline{\tau_w}$ Pa	$-\nabla P$ Pa/m	C_w m/s	R_D kg/m^2·s	E	V_d m/s	d_{30} mm
56	1.20	16.8	0.647	0.53	3 62	0.32	*	*	*	*
56	1.22	20.3	0.414	0.33	329	0.39	*	*	*	*
56	1.23	24.4	0.311	0.63	313	0.45	*	*	*	*
56	1.24	28.1	0.275	1.42	380	0.50	*	*	*	*
56	1.27	31.2	0.266	3.47	538	0.58	*	*	*	*
56	1.28	34.1	0.243	5.27	616	0.63	*	*	*	*
140	1.21	16.5	0.899	0.80	655	0.34	*	0.520	19.8	0.454
140	1.22	20.1	0.745	0.37	664	0.54	0.0293	0.349	24.0	0.374
140	1.24	23.9	0.623	0.77	713	0.66	0.0248	0.213	26.9	0.321
140	1.25	27.8	0.567	2.18	810	0.78	0.0158	0.124	29.5	0.308
140	1.27	31.0	0.504	4.67	945	0.86	0.0079	0.076	32.1	0.310
140	1.30	33.7	0.500	7.47	1,116	0.96	0.0034	0.064	34.5	0.339
280	1.22	16.2	1.045	0.84	885	0.43	*	0.510	20.0	0.599
280	1.24	20.1	0.812	0.42	778	0.65	0.0305	0.434	25.0	0.486
280	1.25	23.5	0.687	1.02	836	0.78	0.0361	0.380	28.5	0.420
280	1.27	27.2	0.635	2.48	922	0.91	0.0519	0.365	31.1	0.383
280	1.31	30.1	0.614	4.41	1,105	0.96	0.0649	0.350	34.2	0.327
280	1.32	33.3	0.559	7.42	1,228	1.00	0.0733	0.325	33.9	0.347
420	1.23	16.0	1.161	1.04	1,043	0.62	*	0.490	20.0	0.729
420	1.24	19.8	0.865	0.58	904	1.00	0.0491	0.466	25.0	0.608
420	1.27	23.1	0.735	1.28	951	1.50	0.0519	0.442	28.8	0.567
420	1.28	26.9	0.683	3.05	1,039	1.70	0.0598	0.434	31.6	0.527
420	1.32	29.7	0.647	5.17	1,209	2.00	0.0688	0.425	34.7	0.494
420	1.35	32.5	0.577	8.25	1,337	2.10	0.0711	0.414	34.5	0.487
560	1.24	15.8	1.213	1.26	1,185	0.79	*	0.460	20.5	0.793
560	1.25	19.5	0.945	0.80	1,047	1.00	0.0541	0.460	25.1	0.772
560	1.28	23.0	0.787	1.57	1,080	1.50	0.0609	0.460	29.6	0.679
560	1.31	26.3	0.715	3.64	1,174	1.80	0.0677	0.460	31.8	0.663
560	1.34	29.2	0.685	5.95	1,343	2.00	0.0857	0.460	34.9	0.612
560	1.38	32.0	0.613	9.43	1,471	2.00	0.0902	0.460	34.8	0.600

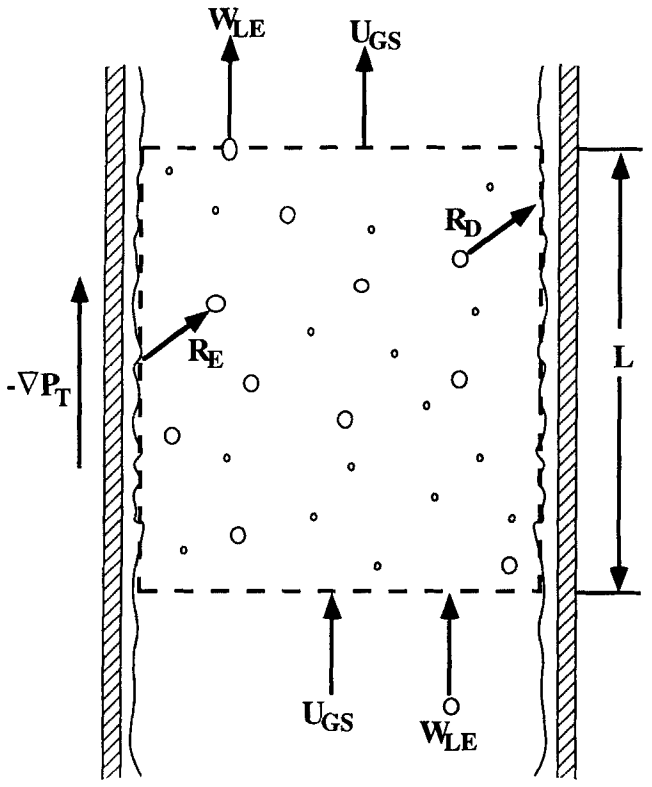

Figure 3. Control volume for momentum balance on the gas droplet core.

friction, ∇P_C is that due to gravity in the gas–droplet core, and ∇P_E is that due to entrainment-deposition (Lopes and Dukler, 1986). Of the four bracketed terms in Eq. 6, the pressure drop, droplet concentration, deposition rate, droplet velocity, and wave velocity have been measured. The fractional contribution of droplet interchange to the measured pressure gradient, $\nabla P_E/\nabla P_T$, is shown in Figure 4. For both fluids, the entrainment contribution increases with gas and liquid flow rates to values as high as 20%.

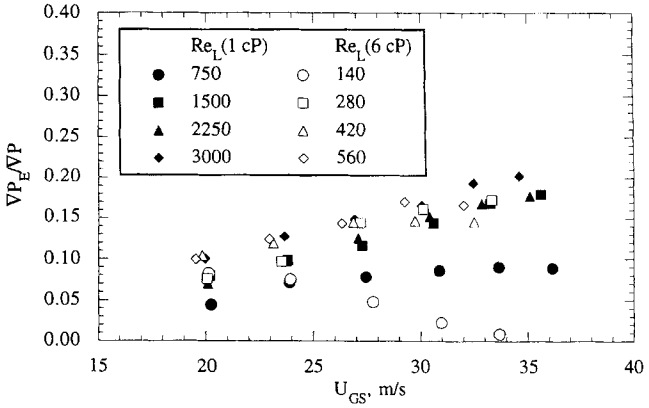

Figure 4. Fractional contribution of entrainment/deposition to the measured pressure gradient.

Overall momentum balance

The control volume for an overall momentum balance is similar to Figure 3, with the tube wall, instead of the interface, as the radial boundary. The terms in this momentum balance differ somewhat from the gas core balance. No mass is transferred through the tube wall, so the convective integral is zero. The surface force integral for this control volume is

$$\int_A T_z \, dA = -\pi DL\tau_w - \pi\frac{D^2}{4}\Delta P. \tag{8}$$

The body force integral, including the liquid film, is

$$\int_V B_z \, dV = -(\rho_G + C_E)g\frac{\pi(D-2m)^2}{4}L - \rho_L gm\pi DL. \tag{9}$$

With these evaluations, Eq. 7 becomes

$$-\frac{\Delta P}{L} = \left\{\frac{4}{D}\tau_w\right\} + \left\{g(\rho_G + C_E)\frac{(D-2m)^2}{D^2} + \frac{4}{D}\rho_L gm\right\}. \tag{10}$$

The bracketed terms are considered two contributions to the total pressure gradient as

$$\nabla P_T = \nabla P_W + \nabla P_G, \tag{11}$$

where ∇P_W is the pressure gradient due to wall friction and ∇P_G is that due to gravity.

Under two conditions aside from negligible experimental error, the total pressure gradient in Eq. 11 should compare closely with the measured pressure gradient. The first condition is equilibrium flow, which was verified experimentally. The second condition is that the momentum transferred during the deposition process is completely absorbed by the liquid film, and is reflected accordingly in the measured wall shear stress and film thickness. Table 4 presents the quantities, $(\nabla P - \nabla P_T)/\nabla P$ and $\nabla P_E/\nabla P$. Under zero-entrainment conditions, ∇P_T and ∇P usually agree within $\pm 5\%$. This result was obtained previously with similar wall shear stress measurements (Govan et al., 1989). However, under entrainment conditions, the measured pressure gradient is usually larger than predicted by Eq. 11, by an amount very similar to the entrainment contribution.

Depositing droplets impinge the film with a significant radial velocity, on the order of 2 m/s (Andreussi and Azzopardi, 1984; Lopes, 1984). A large droplet, relative to the film thickness where it collides, would tend to displace the film initially before coalescing with it. Deceleration then occurs primarily at the wall, resulting in a local, impulsive increase in the wall shear stress at the point of impact. Under this circumstance, little momentum is transferred to the film during deposition. If this occurs often enough, the force at the wall, like the total interfacial force, can be considered the sum of two effects: the continuous stress exerted by the mean film flow and discrete stresses exerted by depositing droplets.

Table 4. Comparison of Overall Momentum Balance with Measured Gradient

Re_L	U_{GS} m/s	∇P_T Pa/m	$(\nabla P - \nabla P_T)/\nabla P$ ×100	$\nabla P_E/\nabla P$ ×100
300	16.5	444	−15.6	0.0
300	20.3	340	−0.9	0.0
300	24.0	338	−9.0	0.0
300	27.6	380	−0.5	0.0
300	31.1	435	−0.2	0.0
300	34.0	492	−0.4	0.0
300	36.5	568	−5.4	0.0
750	16.4	531	−0.6	0.0
750	20.2	439	7.8	4.4
750	23.9	436	5.4	6.9
750	27.4	499	7.9	7.7
750	30.9	564	8.6	8.4
750	33.6	627	8.6	8.9
750	36.2	708	8.3	8.8
1,500	16.3	616	−8.6	0.0
1,500	20.2	529	−2.3	7.7
1,500	23.8	569	7.3	9.6
1,500	27.3	624	11.5	11.5
1,500	30.6	694	12.0	14.2
1,500	33.2	756	13.2	16.6
1,500	35.6	840	10.1	17.8
2,250	16.3	715	−0.4	0.0
2,250	20.1	642	2.3	6.8
2,250	23.7	679	10.2	9.4
2,250	27.1	737	14.2	12.3
2,250	30.4	813	14.4	14.9
2,250	32.8	878	16.3	16.6
2,250	35.1	976	13.6	17.5
3,000	16.2	815	2.7	0.0
3,000	20.0	726	9.0	9.8
3,000	23.7	779	12.4	12.5
3,000	26.9	838	15.7	14.6
3,000	30.0	916	16.7	16.3
3,000	32.5	992	16.9	19.1
3,000	34.6	1,101	13.5	20.0
56	16.8	616	−70.2	0.0
56	20.3	398	−21.0	0.0
56	24.4	332	−6.1	0.0
56	28.1	363	4.5	0.0
56	31.2	517	3.9	0.0
56	34.1	639	−3.7	0.0
140	16.5	862	−31.6	0.0
140	20.1	692	−4.2	8.0
140	23.9	616	13.6	7.3
140	27.8	678	16.3	4.7
140	31.0	819	13.3	2.2
140	33.7	1,036	7.2	0.9
280	16.2	998	−12.8	0.0
280	20.1	759	2.4	7.3
280	23.5	696	16.7	9.4
280	27.2	765	17.0	14.1
280	30.1	898	18.7	15.7
280	33.3	1,087	11.5	16.9
420	16.0	1,119	−7.3	0.0
420	19.8	822	9.1	10.1
420	23.1	762	19.9	11.6
420	26.9	855	17.7	14.1
420	29.7	990	18.1	14.3
420	32.5	1,171	12.4	14.2
560	15.8	1,186	0.0	0.0
560	19.5	913	12.8	9.6
560	23.0	834	22.8	12.0
560	26.3	933	20.5	14.0
560	29.2	1,088	19.0	16.6
560	32.0	1,299	11.7	16.2

The wall shear stress measurements described previously occurred over a very small area, 0.125 mm^2. If depositing drops transfer momentum in the manner described earlier, such a local probe would not experience enough collisions in a finite time to properly record the total wall shear stress. Instead, it would primarily record the continuous stress exerted by the film flow. In this study, the mass-average drop size was comparable to the mean film thickness, and ∇P was larger than ∇P_T by approximately the entrainment contribution. Both are consistent with the mechanism of depositing droplets transferring momentum directly to the tube wall. The momentum from depositing droplets, under the present conditions, is thus not a simple addition to the interfacial friction, in that it does not aid in driving the film upwards.

Conclusions

A series of comprehensive experiments were performed on two gas–liquid systems in upward annular flow. Through core and overall momentum balances, a possible new mechanism for momentum transfer in annular flow has been identified. Measurements are consistent with the idea that depositing droplets displace the film locally, decelerate at the wall, and therefore transfer negligible momentum to the liquid film.

Acknowledgments

This work was made possible by financial support from the Office of Naval Research, under grant N00014-90-J-1090, and the Shell Development Company.

Notation

C_E = entrainment concentration
L = control volume length
r = radial direction in cylindrical coordinates
W_G = gas mass-flow rate
W_{LE} = mass-flow rate of entrainment
z = axial direction in cylindrical coordinates
∇P = measured pressure gradient
μ_L = liquid absolute viscosity
Γ = volume flow per wetted perimeter
ν = liquid kinematic viscosity
ρ_G = gas density
ρ_L = liquid density
τ_w = mean wall shear stress

Literature Cited

Andreussi, P., and B. J. Azzopardi, "On the Entrainment of Drops by the Gas in Two-Phase Annular Flow," *Chem. Eng. Sci.*, **39**(9), 1426 (1984).

Brown, R. C., P. Andreussi, and S. Zanelli, "The Use of Wire Probes for the Measurement of Liquid Film Thickness in Annular Gas-Liquid Flows," *Can. J. Chem. Eng.*, **56**, 754 (1978).

Cousins, L. B., and G. F. Hewitt, "Liquid Phase Mass Transfer in Annular Two Phase Flow: Droplet Deposition and Liquid Entrainment," UKAEA Rep., AERE R5657 (1968).

Dukler, A. E., "The Roll of Waves in Two Phase Flow: Some New Understandings," 1976 Award Lecture, in *Chemical Engineering Education*, p. 108 (1977).

Fore, L. B., "Droplet Entrainment in Vertical Gas-Liquid Annular Flow," PhD Diss., Univ. of Houston, Houston, TX (1993).

Fore, L. B., and A. E. Dukler, "Distribution of Drop Size and Velocity in Gas-Liquid Annular Flow," *Int. J. Multiphase Flow*, **21**, 137 (1995).

Govan, A. H., G. F. Hewitt, D. G. Owen, and G. Burnett, "Wall Shear Stress Measurements in Vertical Air-Water Annular Two-Phase Flow," *Int. J. Multiphase Flow*, **15**(3), 307 (1989).

Hall-Taylor, N. S., G. F. Hewitt, and P. M. C. Lacey, "The Motion and Frequency of Large Disturbance Waves in Annular Two-Phase Flow of Air-Water Mixtures," *Chem. Eng. Sci.*, **18**, 537 (1963).

Hanratty, T. J., and J. A. Campbell, "Measurement of Wall Shear Stress," in *Fluid Mechanics Measurements*, Hemisphere, Washington, DC, p. 559 (1983).

Hewitt, G. F., C. J. Martin, and N. S. Wilkes, "Experimental and Modelling Studies of Annular Flow in the Region Between Flow Reversal and the Pressure Drop Minimum," *PCH PhysicoChem. Hydrodyn.*, **6**(1/2), 69 (1985).

Lopes, J. C. B., "Droplet Sizes, Dynamics and Deposition in Vertical Annular Flow," PhD Diss., Univ. of Houston, Houston, TX (1984).

Lopes, J. C. B., and A. E. Dukler, "Droplet Entrainment in Vertical Annular Flow and Its Contribution to Momentum Transfer," *AIChE J.*, **32**(9), 1500 (1986).

Miner, C. S., and N. N. Dalton, *Glycerol*, Reinhold Publishing, New York (1953).

Miya, M., D. E. Woodmansee, and T. J. Hanratty, "A Model for Roll Waves in Gas-Liquid Flow," *Chem. Eng. Sci.*, **26**, 1915 (1971).

Moeck, E. O., and J. W. Stachiewicz, "A Droplet Interchange Model for Annular-Dispersed Two Phase Flow," *Int. J. Heat Mass Transf.*, **15**, 637 (1972).

Nedderman, R. M., and C. J. Shearer, "The Motion and Frequency of Large Disturbance Waves in Annular Two-Phase Flow of Air-Water Mixtures," *Chem. Eng. Sci.*, **18**, 661 (1963).

Quandt, E. R., "Measurement of Some Basic Parameters in Two-Phase Annular Flow," *AIChE J.*, **11**(2), 311 (1965).

Schadel, S. A., and T. J. Hanratty, "Interpretation of Atomization Rates of the Liquid Film in Gas-Liquid Annular Flow," *Int. J. Multiphase Flow*, **15**(6), 893 (1989).

Schadel, S. A., G. W. Leman, J. L. Binder, and T. J. Hanratty, "Rates of Atomization and Deposition in Vertical Annular Flow," *Int. J. Multiphase Flow*, **16**(3), 363 (1990).

Semiat, R., and A. E. Dukler, "Simultaneous Measurement of Size and Velocity of Bubbles or Drops: A New Optical Technique," *AIChE J.*, **27**(1), 148 (1981).

Zabaras, G., A. E. Dukler, and D. Moalem-Maron, "Vertical Upward Cocurrent Gas-Liquid Annular Flow," *AIChE J.*, **32**(5), 829 (1986).

Manuscript received Mar. 30, 1994, and revision received Oct. 24, 1994.